

Electric-field gradients in Sm_2O_3 , Gd_2O_3 , and Ho_2O_3 measured with perturbed-angular-correlation spectroscopy

J. Shitu,* D. Wiarda, T. Wenzel, M. Uhrmacher, K. P. Lieb, S. Bedi,[†] and A. Bartos
 II. Physikalisches Institut, Universität Göttingen, D-3400 Göttingen, Federal Republic of Germany
 (Received 9 December 1991; revised manuscript received 1 April 1992)

The time-differential perturbed-angular-correlation (PAC) method with ion-implanted ^{111}In tracers was employed to study the hyperfine interactions of ^{111}Cd nuclei in the rare-earth sesquioxides Sm_2O_3 , Gd_2O_3 , and Ho_2O_3 . Up to five electrical quadrupole interactions appeared in each oxide, two of which we attribute to the electric-field gradients (efg) acting on ^{111}Cd on the substitutional lattice sites in the cubic bixbyite phase; in Gd_2O_3 and Sm_2O_3 small fractions can also be related to the B phase. The scaling of the efg in the C phase is discussed in connection with previous findings in other M_2O_3 sesquioxides. A slight linear increase of the quadrupole coupling constants ν_Q for increasing temperature was found.

I. INTRODUCTION

Hyperfine interactions as measured with nuclear magnetic resonance and Mössbauer spectroscopy have been used to elucidate the microscopic environment(s) of constituent or impurity atoms in solids. During the last years, the perturbed-angular-correlation (PAC) technique has developed as a powerful method to investigate metal oxides. Using this method, magnetic and structural phase transitions, oxidation reactions, and the defect chemistry in oxides have been studied.¹⁻⁵ The power of the PAC method in connection with the commonly used ^{111}In radioactive tracers lies in the large quadrupole moment of the 245 keV isomeric state in the daughter nucleus ^{111}Cd . It allows high-precision measurements of the electric-field gradient (efg), which, in oxides, mainly reflect the configurations of the nearest oxygen ions. For this reason, the PAC method is able to sensitively monitor atomic rearrangement and charge- and spin-transfer processes in oxides.

Within the frame of our systematic study of the electric field gradients of ^{111}Cd in oxides with different crystallographic structures,⁶ Bartos *et al.*⁷ have recently reported on the scaling of the efg in a series of binary sesquioxides with bixbyite structure (C phase). This class of oxides may be particularly suitable to study the efg in predominant ionic compounds. First, In_2O_3 shares the bixbyite crystal structure, therefore the other bixbyite matrices are "natural" hosts for the ^{111}In probe. Secondly, the In ion has the smallest radius among the cations forming a cubic C phase, except for Sc. Therefore, the probe can neither be expected to disturb its surrounding by a different type of chemical bonding nor by its size. As the bixbyite oxides M_2O_3 cover a rather wide range of the lattice parameter, one of the motivations for the present work was to extend these studies to the rare-earth oxides Sm_2O_3 , Gd_2O_3 , and Ho_2O_3 , which have even larger lattice parameters than the matrices studied so far.⁷

Properties of the rare-earth oxides have been extensively studied in the past by different experimental methods.⁸⁻¹⁴ The characteristics of the rare-earth

sesquioxides are reviewed in Ref. 15. Up to 2300 K, three polymorphous crystallographic structures have been found (see Fig. 1): the hexagonal-A, monoclinic-B, and cubic-C form (bixbyite).¹⁵ The cubic-C form has space group Ia3; the unit cell contains 48 oxygen atoms and 32 metal atoms, eight of them with D_{3d} point-group symmetry (labeled regular or D site) and 24 with C_2 point-group symmetry (labeled irregular or C site).^{7,15} Hence, two inequivalent cation sites with different octahedral oxygen configurations exist that might be populated by PAC probe atoms. The monoclinic-B form has space group C2/m with 12 metal atoms and 18 oxygen atoms per unit cell; three cation sites exist, among them one with sixfold and one with sevenfold oxygen configuration.

II. THE PAC TECHNIQUE

In a PAC experiment, one measures the perturbation of the angular correlation of a nuclear $\gamma\gamma$ -decay cascade, due to the influence of extranuclear fields. A complete description of the technique can be found in the literature.¹⁶ In the present investigation, we have used the radioactive isotope ^{111}In , which decays by electron capture

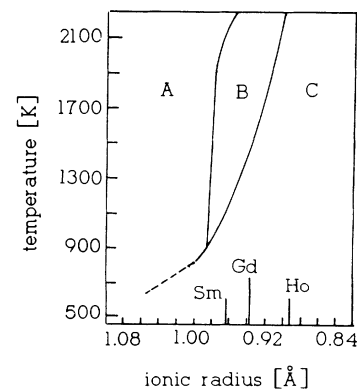


FIG. 1. Structural phase diagram for rare-earth sesquioxides (Ref. 15).

(EC) with a half-life of $T_{1/2}=2.83$ days to the $7/2^+$ state in ^{111}Cd . This excited ^{111}Cd state decays by a two-step γ -ray cascade of 171 and 245 keV. The intermediate $5/2^+$ level is characterized by a half-life of $T_{1/2}=85$ ns, a quadrupole moment of $Q=0.83(13)b$ and a magnetic dipole moment of $\mu_I=-0.766$ magnetons.¹⁷ For $^{111}\text{In}(\text{EC})$ ^{111}Cd and polycrystalline samples the perturbed angular correlation function can be written as an expansion of Legendre polynomials,

$$W(\Theta, t) = 1 + A_{22}G_2(t)P_2(\cos\Theta), \quad (1)$$

with those terms higher than A_{22} neglected, as they are small.¹⁸ Here, Θ denotes the angles between the direction of the emission of the first and the second γ -ray. The perturbation factor $G_2(t)$ depends on the nature of the extranuclear fields and contains the desired information on the hyperfine interaction(s).

The perturbation of the 171–245-keV cascade was measured with a conventional slow-fast set up with four NaI(Tl) detectors in 90° geometry as described in Ref. 19. All 12 possible coincidence combinations of these four detectors were used to generate the experimental perturbation function

$$R(t) = 2 \frac{N(180^\circ, t) - N(90^\circ, t)}{N(180^\circ, t) + 2N(90^\circ, t)} = A'_{22}G_2(t), \quad (2)$$

where, due to the detector geometry,²⁰ the experimental anisotropy A'_{22} is somewhat smaller than the maximum possible value A_{22} .

If only *static* quadrupolar hyperfine interactions are present, $G_2(t)$ for polycrystalline samples is evaluated as¹⁶

$$G_2(t) = \sum_i f_i \sum_n s_{2n}(\eta_i) \exp[-\delta_i t] \cos(\omega_{ni} t) d(\omega_{ni}, \tau_r). \quad (3)$$

The quantities f_i denote the relative fractions of the probe nuclei that are subject to the efg i , which is characterized by the coupling constant ν_{Qi} , the asymmetry parameter η_i , and the distribution width δ_i . For each hyperfine interaction the coupling constant and the asymmetry parameter are related to the components V_{xx} , V_{yy} , and V_{zz} of the diagonalized efg tensor via the relations

$$\nu_Q = eQV_{zz}/h, \quad \eta = (V_{xx} - V_{yy})/V_{zz}, \quad (4)$$

where $|V_{xx}| \leq |V_{yy}| \leq |V_{zz}|$. As can be seen in (3), the $R(t)$ pattern related to a single efg contains three transition frequencies

$$\omega_n = g_{2n}(\eta)\nu_Q, \quad n = 1, 2, 3, \quad (5)$$

which can be resolved by a Fourier transformation. Expressions for the functions $g_{2n}(\eta)$ and $s_{2n}(\eta)$ can be found in Ref. 21. Random lattice distortions or distant lattice defects cause a distribution of similar efg's. This leads to a damping of the $R(t)$ pattern that can be described with a Lorentzian term with the distribution width δ . The damping due to the finite time resolution of the PAC setup, $\tau_r = 3.0(5)$ ns, of the detectors was taken into account by the factor²²

$$d(\omega_n, \tau_r) = \exp[-(\omega_n \tau_r)^2 / 16 \ln 2]. \quad (6)$$

III. TARGET PREPARATION AND ^{111}In IMPLANTATION

Ho_2O_3 , Sm_2O_3 , and Gd_2O_3 powder samples were commercially obtained (Alpha-Products, purity: 99.999%). X-ray analyses of the samples verified that Ho_2O_3 was present in the pure C phase, while Sm_2O_3 and Gd_2O_3 were present in a mixture of roughly 85% C and 15% B phase. The oxide powders were rolled onto silver backings to become mechanically stable for implantation. About 10^{12} $^{111}\text{In}^+$ ions were implanted at 400 keV by means of the Göttingen ion implanter IONAS.²³ In order to remove radiation damage, the samples (Sm_2O_3 and Gd_2O_3) were heated for $t=1$ h at a pressure of $p=10^{-5}$ mbar at $T=1023$ K. In the case of Ho_2O_3 , annealing was done at 673 K at a pressure of $p=3 \times 10^{-2}$ mbar (sample I) or no annealing of the radiation damage was carried out (sample II). Afterwards, all PAC measurements were performed at different temperatures T_m either in air or at pressures of 3×10^{-2} or 10^{-5} mbar.

To obtain Sm_2O_3 in the pure B phase, ^{111}In was implanted into the original powder (mixture of C and B phase), which was afterwards heated for $t=20$ h at $T=1425$ K in air. X-ray analysis confirmed a complete transition to B phase Sm_2O_3 .

IV. EXPERIMENTAL RESULTS

A. The C-form sesquioxides

Figures 2 and 3 display $R(t)$ patterns for ^{111}Cd in Sm_2O_3 and Ho_2O_3 taken at the indicated temperatures. Figure 4 shows the development of the perturbation function for ^{111}Cd in Gd_2O_3 with the measuring temperature T_m . Up to six different hyperfine (hfi) components in each matrix were needed to describe the experimental data; the resulting efg parameters are summarized in Table I. An overview of the evolution of all observed fractions f_i with the measuring temperature T_m is shown in Figs. 5(a)–5(d) for Sm_2O_3 , Gd_2O_3 , and Ho_2O_3 (sample I: annealed; sample II: not annealed).

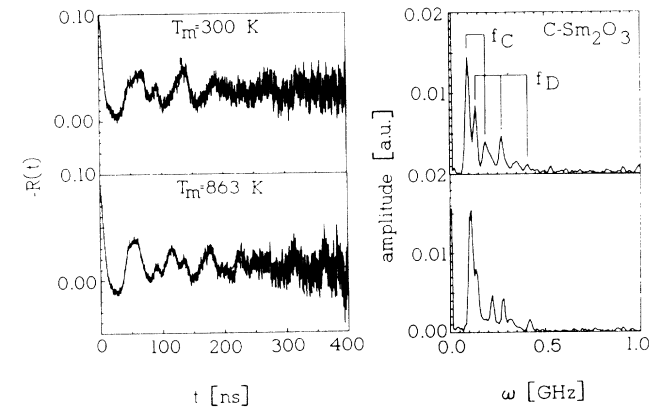


FIG. 2. Perturbation functions $R(t)$ and Fourier spectra (right-hand side) taken for ^{111}Cd impurities in Sm_2O_3 at measuring temperatures $T_m = 300$ and 863 K.

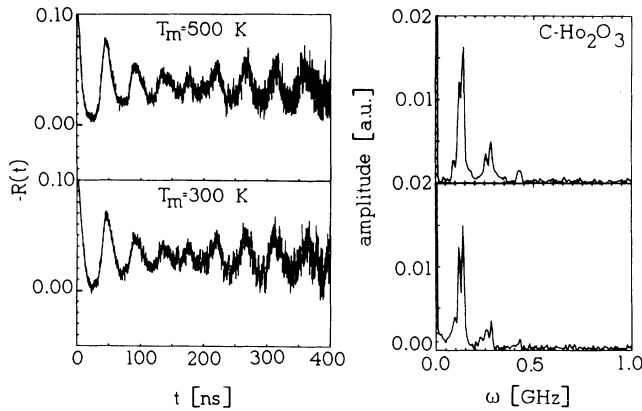


FIG. 3. Same as Fig. 2, for ^{111}Cd in Ho_2O_3 .

1. The strongly populated hfi

In all investigated samples about 70–80% of the probe atoms are subject to two well-defined quadrupole interactions. The corresponding transition frequencies ω_n are indicated in one of the Fourier transforms shown in Fig. 2. In analogy to our previous work^{6,7} on ^{111}In -doped In_2O_3 , Sc_2O_3 , Y_2O_3 , Yb_2O_3 , and Sc_2O_3 and for the reasons outlined in Sec. V, we label these two sites as “C” (asymmetric site: $\eta \approx 0.8-1$) and “D” (symmetric site: $\eta \approx 0$). The development of these two fractions as a function of T_m as depicted in Fig. 5 only shows a weak temperature dependence. As seen in many ^{111}In -doped oxides, narrowing of the frequency distribution with increasing measuring temperature is observed. Furthermore, both coupling constants ν_{QC} and ν_{QD} increase linearly with increasing measuring temperature T_m , as shown in Fig. 6.

2. The weakly populated sites

In addition to the strongly populated sites C and D, several weakly populated hyperfine fractions were found in the PAC spectra. In the following sections, we describe the observed behavior of these smaller fractions.

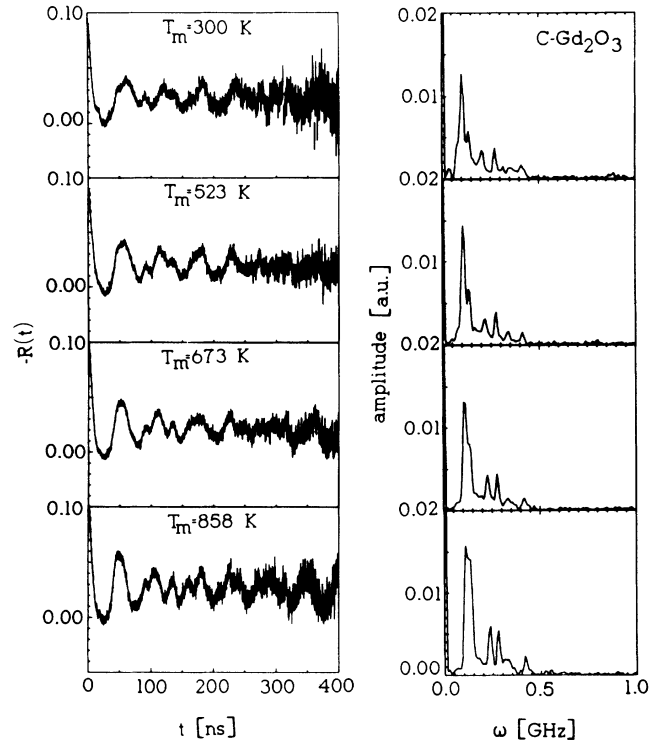


FIG. 4. Development of the perturbation functions and their Fourier spectra with the measuring temperature T_m for ^{111}Cd in Gd_2O_3 .

Similar hfi parameters are labeled with the same index. These additional fractions will also be interpreted in Sec. V.

3. Fraction 3

In nearly all perturbation functions of the three oxides, a similar efg distribution ($\delta \approx 20$ MHz) centered around $\nu_Q = 165$ MHz, $\eta \approx 0.4$ was observed. In Sm_2O_3 , this fraction remained fairly constant at $f_3 \approx 15\%$. In Gd_2O_3 , this situation is less clear, as the fraction f_3 disappears at 400 K, while a new fraction f_3 , with hyperfine parameters $\nu_{Q3} = 120(9)$ MHz, $\eta_3 = 0.75(4)$, and $\delta_3 = 14(3)$

TABLE I. Summary of hfi parameters for ^{111}Cd in Ho_2O_3 , Gd_2O_3 , and Sm_2O_3 .

	Ho_2O_3			Gd_2O_3			Sm_2O_3		
	ν_Q (MHz)	δ (MHz)	η	ν_Q (MHz)	δ (MHz)	η	ν_Q (MHz)	δ (MHz)	η
C	81(1)	3(1)	0.83(2)	63(3)	4(1)	0.97(3)	59(2)	4(1)	0.91(3)
D	150(2)	2(2)	0	145(4)	3(1)	0	144(1)	5(1)	0
3	175(10)	23(5)	0.4(1)	167(6)	17(6)	0.45(7)	175(15)	20(7)	0.4(2)
4				208(12)	21(6)	> 0.96	210(10)	22(4)	> 0.95
5	86(9)	6(2)	< 0.2	93(6)	4(3)	0.2(1)			
B				209(1) ^a	2.0(5)	1.0	208(1)	3.0(5)	0.98(1)

^aReference 29.

MHz is found for $T_m \geq 673$ K.

In the first Ho_2O_3 sample (I), fraction f_3 was present with a nearly constant population and very similar hyperfine parameters at all temperatures T_m . In the second Ho_2O_3 sample (II), which had not been annealed,

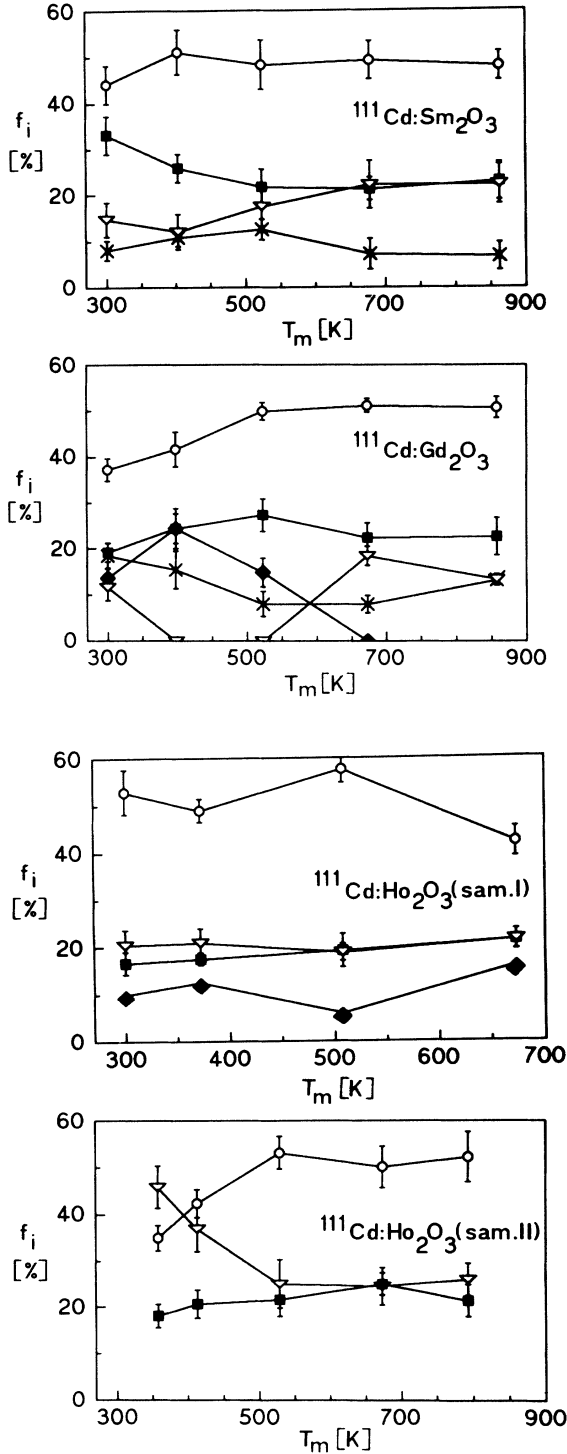


FIG. 5. Evolution of the hyperfine fractions f_i ($i=1-5$) found in Sm_2O_3 , Gd_2O_3 , and Ho_2O_3 with the measuring temperature T_m . The symbols are as follows: \circ f_c , \blacksquare f_D , ∇ f_3 , \times f_4 , \blacklozenge f_5 .

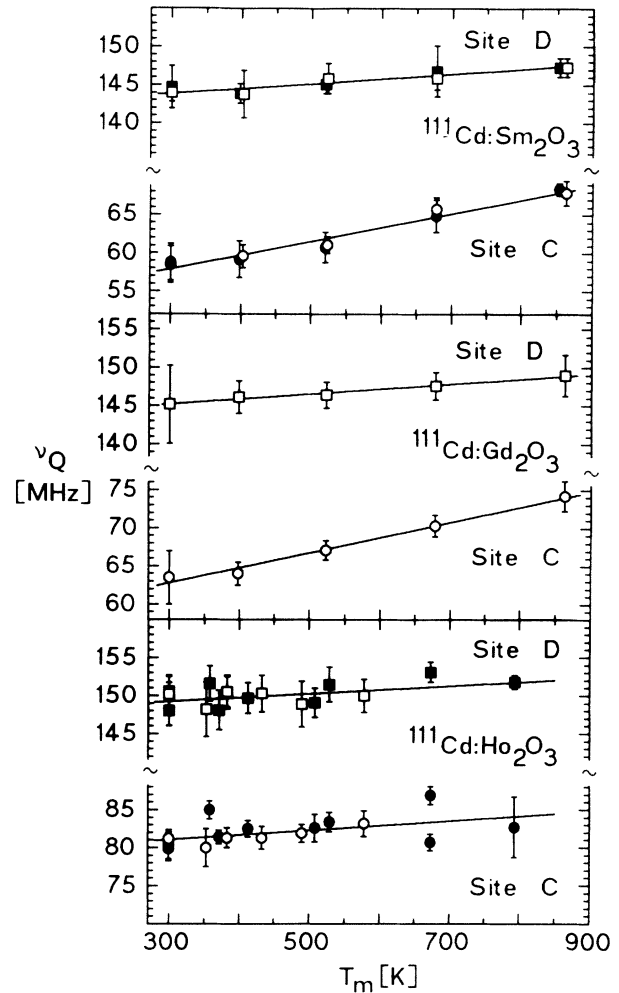


FIG. 6. Measured temperature dependence of the quadrupole coupling constants ν_{QC} and ν_{QD} in Sm_2O_3 , Gd_2O_3 , and Ho_2O_3 . The open symbols refer to PAC measurements in air, the dots to measurements *in vacuo*.

the population of f_3 decreased from $f_3=46(5)\%$ at $T_m=358$ K to $f_3=25(5)\%$ at $T_m=529$ K and then stayed constant up to $T_m=793$ K. During these PAC measurements the pressure was 10^{-5} mbar. On the contrary, a sample annealed in vacuum at 873, 963, and 1023 K showed this fraction f_3 to be quenched to 6%. A final measurement in air at 450 K removed this fraction completely.

4. Fraction 4

In Sm_2O_3 and Gd_2O_3 , a hfi with a population of $f_4 \approx 10\%$ and parameters, as given in Table I was observed, which showed no significant temperature dependence.

5. Fraction 5

The interaction labeled f_5 appeared only in the annealed Gd_2O_3 and Ho_2O_3 samples. In Gd_2O_3 , fraction f_5 increased to 25% at $T_m=407$ K, correlated with a de-

crease of f_3 . At higher temperatures ($T_m > 650$ K), f_5 vanished in favor of f_3 . In Ho_2O_3 , the fraction $f_5 \approx 12\%$ was only found in sample I at elevated temperatures in air after a vacuum annealing at 1023 K had been carried out. As the fractions f_5 have small distribution widths $\delta_5 \leq 6$ MHz in the various samples, they represent well-defined probe sites.

B. $\text{B-Sm}_2\text{O}_3$

Figure 7 shows the experimental $R(t)$ patterns for ^{111}Cd in $\text{C-Sm}_2\text{O}_3$ (at the top) in comparison with those in $\text{B-Sm}_2\text{O}_3$ taken at 473 and 873 K. In the B phase, a single, well-defined quadrupole interaction labeled "B" is observed with hyperfine parameters given in Table I. Note that the C-phase Sm_2O_3 sample contained few percent of the B phase as verified by X-ray diffraction and the agreement of ν_{QB} and ν_{Q4} . In contrast to the hfi observed in the C phase of Sm_2O_3 , the coupling constant ν_{QB} was found to decrease²⁴ with increasing temperature T_m . Furthermore, the asymmetry parameter converges to $\eta_B = 1$ at high temperatures.²⁴

V. DISCUSSION

A. Substitutional sites C and D

In close analogy to Ref. 7 we attribute the two efg's "C" and "D" to the two possible substitutional cation sites in the bixbyite structure. The following arguments support this interpretation: In spite of small, but systematic changes of both quadrupole interactions with T_m , the two efg's are observed over the whole range of measuring temperatures. As explained in the introduction, two different cubic oxygen octahedra exist around each cation in the cubic-C form: a highly symmetric one

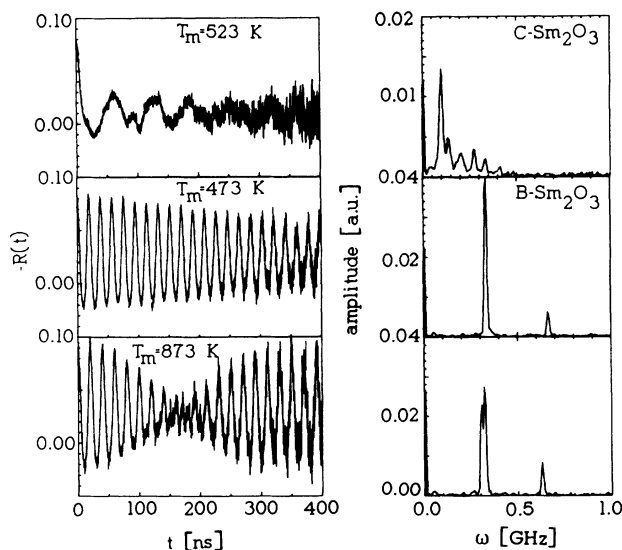


FIG. 7. Perturbation functions $R(t)$ and their Fourier spectra of Sm_2O_3 (C phase, top) as compared to the PAC data in Sm_2O_3 (B phase) taken at $T_m = 473$ and 873 K.

around site D and a strongly distorted one around C. The point-charge model (PCM) predicts $\eta_D = 0$ and $\eta_C \approx 0.8$ for the two sites in agreement with the experimental values. The relative population of the two sites in the bixbyite structure is $f_C/f_D = 3$ if both sites are occupied with equal probability. This was verified for In_2O_3 , where the tracer element and the cations of the lattice are identical.⁶ In the present experiment, the experimental ratio f_C/f_D is smaller than 3.0 in most cases, with the C site being less populated. A similar behavior has also been observed in our previous studies of the other bixbyite oxides.⁷

1. Scaling of the electric-field gradients

It is well known that the bonding in these sesquioxides is mainly ionic.²⁵ Under such conditions the efg acting on probe nuclei on substitutional sites should scale linearly with a^{-3} where a is the lattice constant. In Fig. 8 the coupling constants ν_Q of both sites C and D and the asymmetry parameter η_c are plotted vs a^{-3} , including the values for the bixbyite oxides reported in Ref. 7 (Dy_2O_3 , Y_2O_3 , Yb_2O_3 , and Sc_2O_3) and Ref. 6 (In_2O_3). The new data agree perfectly with the values presented in Ref. 7: We find a nearly linear dependence of ν_{QC} with a^{-3} for the low-symmetry C site and nearly constant values of ν_{QD} at the D site. For this site, no deviation from axial symmetry is found ($\eta_D = 0$), which is in good agreement with the regular oxygen octahedron at site D. On the other hand, the increase of η_c with increasing lattice constant indicates that the irregular octahedron

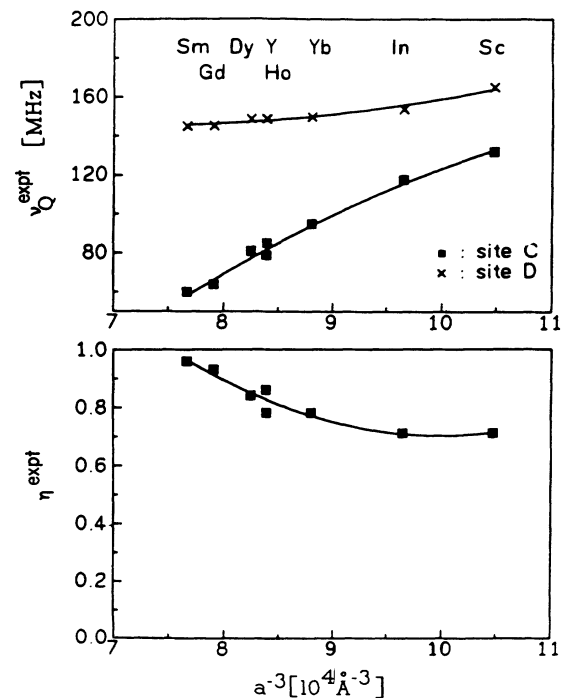


FIG. 8. Observed quadrupole frequencies ν_{QC} and ν_{QD} and asymmetry parameter η_c for substitutional ^{111}Cd impurities plotted vs a^{-3} , a being the lattice parameter. The results of Refs. 6 and 7 have been included.

changes its configuration through the series. Such behavior was also found in precise X-ray-diffraction measurements and therefore does not appear to be induced by the ^{111}Cd impurity.

2. Temperature dependence of the efg

The evolution of the coupling constant for both structural sites *C* and *D* with the measuring temperatures T_m was displayed in Fig. 6. Within the errors, the temperature dependence of the coupling constants ν_{QC} and ν_{QD} is linear in T_m :

$$\nu_Q(T_m) = \nu_{Q0}(1 + bT_m). \quad (7)$$

In Ho_2O_3 , Gd_2O_3 , and Sm_2O_3 the increase is more pronounced for the *C* site than for the *D* site. Figure 9 compares the slope parameter b for these oxides. For the symmetric site *D* a constant value of b is found for all oxides, while for the *C* site b increases by a factor of 7 between Sc_2O_3 and Sm_2O_3 . In all cases the b values are positive. A simple PCM calculation with temperature-dependent lattice constants^{26,27} predicts negative b values as the lattice widens. On the other hand, the temperature dependence of efg's in semiconducting materials is not understood at all and at present we cannot relate the observed variation of b to physical properties of these oxides.²⁸

B. Other efg components

As mentioned before, additional (small) fractions were needed to fit all PAC spectra, some of them have also been found in our previous PAC measurements in bixbyite oxides.⁷ We will discuss them in the following, starting with the most evident interpretations.

1. Fraction f_3

The efg distribution labeled f_3 was found in all samples. These hfi parameters are quite similar to those found in Ref. 7. There, the ratio $(f_c + f_3)/f_D$ was found to be close to 3. This ratio would be expected if the two substitutional *C* and *D* sites are populated with equal probability. It was suggested that f_3 represents ^{111}In probes on the *C* site having trapped a lattice defect. Al-

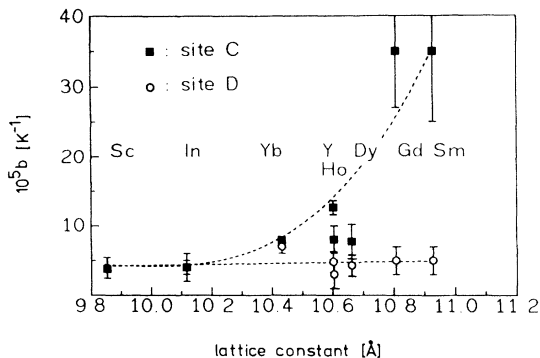


FIG. 9. Slope parameter b taken from the linear temperature dependence of the coupling constants ν_Q at the *C* and *D* site, plotted vs the lattice constant a .

though, in the present data, the temperature dependence of f_3 is less obvious, the ratio $(f_c + f_3)/f_D$ approaches 3 for increasing measuring temperature. Therefore, we adopt the previous interpretation of this fraction and relate it to probes substituted at a defective *C* site. When comparing the ν_{Q3} values in the various matrices studied, no correlation with the lattice constant is found, in contrast to the efg at sites *C* and *D*. This points to a ^{111}In -specific complex. But additional experiments have to be done to clarify the origin of f_3 .

2. Fraction f_5

A similar argumentation is valid for this hfi. As no dependence of the hyperfine parameters on the lattice constant was found, we also suggest the formation of a probe-specific complex.

3. Fraction f_4

This hfi is attributed to substitutional ^{111}In located in B-phase contaminations in $\text{C-Sm}_2\text{O}_3$ and $\text{C-Gd}_2\text{O}_3$. This is confirmed by comparing the hyperfine parameters of fraction f_4 with those of ^{111}Cd in pure $\text{B-Sm}_2\text{O}_3$ and $\text{B-Gd}_2\text{O}_3$, labeled "B" in Table I. Furthermore, the amount of the B-phase component derived from X-ray analysis ($\approx 15\%$) is close to the PAC fraction $f_4 \approx 10\%$ and supports this interpretation.

VI. CONCLUSIONS

In this study we investigated the electric hyperfine interactions of ^{111}Cd impurities in the three bixbyite oxides Sm_2O_3 , Gd_2O_3 , and Ho_2O_3 . Including the previous results of Bartos *et al.*,⁷ we now can compare a set of eight oxides having the same crystalline structure, but differing in their lattice constant by some 10%. After implantation of the ^{111}In probes and subsequent high-temperature annealing, all these oxides show a common behavior: Besides small amounts of probes in different phases and/or with uncorrelated damage, about 80% of the PAC probes occupy two sites, which have been identified as the two possible substitutional cation sites of bixbyite structure. At both sites the cations are enclosed in an oxygen octahedron; the regular one (*D*) stays unchanged in shape, and is less affected by the changing lattice parameter and measuring temperature. The irregular one (*C*) exhibits systematic variations of the efg parameters, while changing the lattice parameter and indicates distortions of the oxygen octahedron. Furthermore, the efg at this site increases linearly with the measuring temperature. The temperature dependence of these efg's turned out to be similar than dependence in other semiconducting compounds.

ACKNOWLEDGMENTS

We are indebted to A. Pasquevich for several discussions and to D. Purschke and L. Ziegeler for their help with the ^{111}In implantations. This work has been supported by Deutsche Forschungsgemeinschaft and Stiftung Volkswagenwerk.

- *On leave of absence from Departamento de Física, Facultad de Ciencias Exactas, Universidad Nacional de La Plata, La Plata, Argentina.
- †Permanent address: Department of Physics, Panjab University, Chandigarh, India.
- ¹M. Forker and H. Hammesfahr, *Z. Phys.* **260**, 261 (1973).
- ²A. Bartos, M. Uhrmacher, K. P. Lieb, and W. Bolse, *Hyperfine Interact.* **50**, 619 (1989).
- ³A. F. Pasquevich, A. G. Bibiloni, C. P. Massolo, and A. Lopez-Garcia, *Phys. Lett.* **82A**, 34 (1981).
- ⁴A. Bartos, W. Bolse, K. P. Lieb, and M. Uhrmacher, *Phys. Lett. A* **130**, 177 (1988); M. Uhrmacher, A. Bartos, and W. Bolse, *Mater. Sci. Eng. A* **116**, 129 (1989).
- ⁵F. Requejo, A. G. Bibiloni, H. Saitovich, and P. R. J. Silva, *Phys. Status Solidi A* **120**, 105 (1990).
- ⁶W. Bolse, M. Uhrmacher, and K. P. Lieb, *Phys. Rev. B* **36**, 1818 (1987); W. Bolse, M. Uhrmacher, and J. Kesten, *Hyperfine Interact.* **35**, 931 (1987).
- ⁷A. Bartos, K. P. Lieb, A. F. Pasquevich, and M. Uhrmacher, *Phys. Lett. A* **157**, 513 (1991).
- ⁸H. B. Lal, *J. Phys. C* **13**, 3969 (1980).
- ⁹V. Pratap, B. K. Kerma, and H. B. Lal, *Proc. Nat. Acad. Sci. India* **48A**, 20 (1978).
- ¹⁰A. Fert, *Bull. Soc. Franc. Miner.* **85**, 267 (1962).
- ¹¹M. Foex and J. P. Traverse, *Bull. Soc. Franc. Miner.* **89**, 184 (1966).
- ¹²Eyring LeRoy, in *Heterogeneous Kinetics at Elevated Temperatures*, edited by G. R. Belton and W. Worrell (Plenum, New York, 1970).
- ¹³M. V. Rhyzkov, V. A. Gubanov, Yu. A. Teterin, and A. S. Baev, *Z. Phys. B* **59**, 7 (1985).
- ¹⁴M. Urban and B. C. Cornilsen, *J. Phys. Chem. Solids* **48**, 475 (1987).
- ¹⁵Eyring LeRoy, *The Binary Rare Chemistry of Rare Earths*, edited by K. A. Gschneider and L. Eyring (North-Holland, Amsterdam, 1979), p. 337.
- ¹⁶See, for example, H. Frauenfelder and R. M. Steffen, in *Alpha, Beta, and Gamma Ray Spectroscopy*, edited by K. Siegbahn (North-Holland, Amsterdam, 1967), pp. 967 and 1182.
- ¹⁷R. Vianden, *Hyperfine Interact.* **15/16**, 1081 (1983).
- ¹⁸S. Raman and H. J. Kim, *Nucl. Data Sheets* **6**, 39 (1971).
- ¹⁹A. R. Arends, C. Hohenemser, F. Pleiter, H. de Waard, I. Chow, and R. M. Suter, *Hyperfine Interact.* **8**, 191 (1980).
- ²⁰M. J. Yates, in *Alpha, Beta, and Gamma Ray Spectroscopy*, edited by K. Siegbahn (North-Holland, Amsterdam, 1967).
- ²¹J. Kaifosz (unpublished); L. A. Mendoza-Zelis, A. G. Bibiloni, M. C. Larocoche, A. R. Lopez-Garcia, J. A. Martinez, R. C. Mercader, and A. F. Pasquevich, *Hyperfine Interact.* **3**, 315 (1977).
- ²²J. D. Rogers and A. Vazquez, *Nucl. Instrum. Methods* **130**, 539 (1975).
- ²³M. Uhrmacher, K. Pampus, F. J. Bergmeister, D. Purschke, and K. P. Lieb, *Nucl. Instrum. Methods B* **9**, 234 (1985).
- ²⁴J. Shitu (unpublished).
- ²⁵B. M. Angelov, *J. Phys. C* **15**, L239 (1982).
- ²⁶R. W. G. Wyckoff, *Crystal Structures* (Interscience, London, 1965), Vol. 1.
- ²⁷S. Stechura and W. J. Campbell, *U. S. Bur. Mines Rep. Invest.* **47**, 5847 (1961).
- ²⁸G. Gashurov and O. J. Sovers, *Acta Crystallogr. B* **26**, 938 (1970).
- ²⁹D. Lupascu (private communication).